

Unique dynamics and exocytosis of single inhibitory synaptic vesicles

Chungwon Park^a, Xingxiang Chen^a, Chong-Li Tian^{b, c}, Gyu Nam Park^{d, e}, Nicolas Chenouard^f, Hunki Lee^{a, g}, Xin Yi Yeo^{h, i}, Sangyong Jung^{h, j}, Guoqiang Bi^{b, c}, Richard W. Tsien^k, and Hyokeun Park^{a, l, m, 1}

^aDivision of Life Science

The Hong Kong University of Science and Technology, Clear Water Bay, Kowloon, Hong Kong

^bSchool of Life Sciences, University of Science and Technology of China, Hefei, Anhui, China

^cChinese Academy of Sciences, Key Laboratory of Brain Function and Disease, University of Science and Technology of China, Hefei, Anhui, China

^dDepartment of Chemistry Chung-Ang University, Seoul 06974, Korea

^eCreative Research Initiative Center for Chemical Dynamics in Living Cells, Chung-Ang University, Seoul 06974, Korea

^fUniv. Bordeaux, CNRS, Interdisciplinary Institute for Neuroscience, IINS, UMR 5297, F-33000 Bordeaux, France

^gCiM-IMPRS Joint Graduate Program,

Institut fuer Medizinische Physik und Biophysik,

Westfaelische Wilhelms-Universitaet Muenster, Muenster, Germany

^hSingapore Bioimaging Consortium, Agency for Science, Technology and Research,

11 Biopolis Way, Singapore

ⁱDepartment of Psychological Medicine, Yong Loo Lin School of Medicine,

National University of Singapore, Singapore

^jDepartment of Physiology, Yong Loo Lin School of Medicine, National

University of Singapore, Singapore

^kNYU Neuroscience Institute and Department of Physiology and Neuroscience,

New York University, New York, NY, USA

^lDepartment of Physics,

The Hong Kong University of Science and Technology, Clear Water Bay, Kowloon,

Hong Kong

^mState Key Laboratory of Molecular Neuroscience

The Hong Kong University of Science and Technology, Clear Water Bay, Kowloon,

Hong Kong

¹To whom correspondence should be addressed. Email: hkpark@ust.hk

Classification

Biological Sciences, Neuroscience

Key words

Inhibitory synaptic vesicles; Exocytosis; release probability; three-dimensional

45 tracking; real-time imaging

46

47 **Author Contributions**

48 C.P. and H.P. designed the experiments. C.P., X.C., and C.-L.T., performed the

49 experiments. C.P., C.-L.T., G.N.P., N.C., and HL analyzed data. C.P., C.-L.T., X.Y.Y.,

50 S.J., G.B., R.W.T., and H.P. discussed and interpreted results, C.P., X.C., C.L.T., S.J.,

51 R.W.T., and H.P. wrote the manuscript. S.J., G.B., and H.P. supervised students.

52

53

54 **This PDF file includes:**

55 Main Text

56 Figures 1 to 5

57

Abstract

The balance between excitation and inhibition is essential for maintaining proper brain function in the central nervous system. Inhibitory synaptic transmission plays an important role in maintaining this balance. Inhibitory synaptic transmission faces greater kinetic demands than excitatory synaptic transmission, yet remains less well understood. In particular, the dynamics and exocytosis of single inhibitory vesicles have not been investigated due to both technical and practical limitations. Using quantum dots (QDs)-conjugated antibodies against the luminal domain of the vesicular GABA transporter (VGAT) to selectively label single GABAergic inhibitory vesicles and dual-focus imaging optics, we tracked single inhibitory vesicles up to the moment of exocytosis (i.e., fusion) in three dimensions in real time. Using three-dimensional trajectories, we found that the total travel length before fusion of inhibitory synaptic vesicles was smaller than that of synaptotagmin-1 (Syt1)-labeled vesicles. Fusion times of inhibitory vesicles were shorter compared with those of Syt1-labeled vesicles. We also found a close relationship between release probability to the proximity to fusion sites and total travel length of inhibitory synaptic vesicles. Furthermore, inhibitory synaptic vesicles exhibited a higher prevalence of kiss-and-run fusion than Syt1-labeled vesicles. Thus, our results showed that inhibitory synaptic vesicles have the unique dynamics and fusion properties that facilitate their ability to support fast synaptic inhibition.

Significance

Despite of its importance, the dynamics of single inhibitory synaptic vesicles before exocytosis has not been investigated. Here, we tracked single inhibitory vesicles up to the moment of exocytosis in three dimensions in real time using QDs-conjugated antibodies against the luminal domain of the vesicular GABA transporter (VGAT). We found that inhibitory synaptic vesicles had smaller total travel length before fusion, shorter fusion time and a higher prevalence of kiss-and-run than synaptotagmin-1-labeled vesicles. For the first time, we showed the unique dynamics and exocytosis of single inhibitory synaptic vesicles before exocytosis, which supports fast inhibitory synaptic transmission. Thus, our results suggest that unique dynamics and exocytosis of inhibitory synaptic vesicles is an important factor in inhibitory synaptic transmission.

Introduction

Neurons communicate with other neurons and different types of cells by releasing neurotransmitters in presynaptic terminals through exocytosis, and subsequently activating receptors in postsynaptic terminals (1-4). The central synapses can be broadly classified into excitatory or inhibitory synapses, depending on the types and effects of neurotransmitters they release. While the excitatory synapses act to generate, propagate and potentiate neuronal responses for information processing (5), the inhibitory synapses are essential for feedback or feedforward inhibition to control neural excitability (6). Inhibitory synaptic transmission, which is mediated primarily through the release of GABA in the central nervous system, coordinates the pattern of excitation and synchronization of the neuronal network to regulate neuronal excitability (7, 8). Thus, the tight regulation of both excitatory and inhibitory neurotransmission is essential for the proper functions of the brain.

The systematic analysis of the components and molecular events of vesicle fusion and neurotransmitter release has generated general models for the organization and functional operation of the pre- and postsynaptic components of synapses (9-11). The high local Ca^{2+} concentration due to activity-induced activation of Ca^{2+} channels triggers the local buckling of the plasma membrane through the direct interaction between the C2B domain of synaptotagmin-1 (Syt1) and the lipid on the membrane (12-14). This leads to synchronous fusion of the membrane and the release of its content into the synaptic cleft (15). Once released, the excitatory and inhibitory

neurotransmitters exert their respective effects through glutamate or GABA receptors on the postsynaptic membrane.

The generalized understanding of vesicular release built on excitatory neurotransmission is not able to explain distinct inhibitory synaptic transmission. The size of the readily releasable pool (RRP) of synaptic vesicles in the striatal inhibitory GABAergic neurons, probed by the use of hypertonic sucrose solution, is three times higher than that of excitatory hippocampal glutamatergic neurons (16). Furthermore, the average vesicular release probability and number of release sites of the inhibitory neurons are higher than those of excitatory neurons (16-18). These results suggest at least quantitative differences in properties of vesicle release and recycling in the GABAergic synapses. In addition, the disproportionate effects of the knockout of the individual or all synapsin genes between the two types of synapses, provide a molecular perspective on the potential differences between excitatory and inhibitory synapses (20-23).

Despite the crucial roles of inhibitory synaptic vesicles in information processing in the neuronal network, the dynamics of the inhibitory synaptic vesicles in presynaptic terminals is poorly understood. In particular, the real-time dynamics of single inhibitory synaptic vesicles in hippocampal neurons upon stimulation have not been investigated due to technical and practical limitations, including the lack of specific single inhibitory vesicular markers, the structural complexity of synapses in three dimensions, and the extreme small size of synaptic vesicles (diameter of 40–50 nm, which is well below the resolution of conventional light microscopy)(2).

Here, we report the real-time three-dimensional tracking of single inhibitory synaptic vesicles in dissociated hippocampal neurons using dual-focus optics and QD-conjugated antibodies against the luminal domain of the vesicular GABA transporter (VGAT) to selectively label single GABAergic vesicles. We found that fusion times of inhibitory vesicles were significantly shorter than those of Syt1-labeled vesicles and the total travel length before fusion of inhibitory vesicles was smaller compared with the Syt1-labeled vesicles. The release probability of inhibitory synaptic vesicles was closely correlated to the proximity to fusion sites and the total travel length before fusion. Inhibitory synaptic vesicles exhibited a higher prevalence of kiss-and-run fusion compared with Syt1-labeled vesicles. Thus, our results indicate that inhibitory synaptic vesicles have unique dynamics and fusion properties.

Results

Real-time three-dimensional tracking of single inhibitory synaptic vesicles in hippocampal neurons

In order to study the dynamics of single inhibitory synaptic vesicles in mature synapses, we tracked single inhibitory synaptic vesicles in three dimensions in real time up to the moment of exocytosis in mature dissociated hippocampal neurons (i.e., days in vitro (DIV) 14 – 21) similar to the previous method used in the tracking of single synaptic vesicles (24) of undetermined identity. We previously reported the real-time three-dimensional tracking of single synaptic vesicles loaded with a streptavidin-conjugated quantum dots (QDs)-conjugated to biotinylated antibodies against the

luminal domain of endogenous synaptotagmin-1 (Syt1) (or Syt1-labeled synaptic vesicles) with an accuracy of 20 to 30 nanometers (less than the synaptic vesicle diameter) in neurons (24). In order to specifically label inhibitory synaptic vesicles with QDs in living hippocampal neurons, we conjugated streptavidin-coated QDs with a commercially available biotinylated antibody which is specific to the luminal domain of the endogenous vesicular GABA transporter (VGAT, also termed vesicular inhibitory amino acid transporter (VIAAT))(Fig. 1A). The QDs-conjugated antibodies bind to the luminal domain of VGAT, exposed after exocytosis during electrical stimulation. CypHer5E-labeled antibodies against the luminal domain of VGAT (VGAT-CypHer5E - a fluorescent marker that selectively labels inhibitory synaptic vesicles (25)) were used to label spontaneously released inhibitory synaptic vesicles during 2 hours of incubation in order to locate the inhibitory presynaptic terminals. The colocalization between fluorescence signals of QDs and VGAT-CypHer5E shown in Fig. 1B indicates that QDs-conjugated antibodies against VGAT successfully labeled inhibitory synaptic vesicles in the inhibitory presynaptic terminals marked by VGAT-CypHer5E. Only colocalized QD-labeled synaptic vesicles were used for data analysis. Exocytosis of single QD-loaded vesicles was reflected by a sudden irreversible drop in the fluorescent signal caused by the quenching of exposed QD by extracellular trypan blue (extracellular quencher) (24). The positions of single synaptic vesicles loaded with QDs in the x-y plane were localized with an accuracy of tens of nanometers using a technique called fluorescence imaging with one nanometer accuracy (FIONA)(24, 26, 27). The z-positions of single vesicles loaded with QDs were localized with an accuracy of tens of

nanometers using dual-focusing imaging optics (24, 28). Using these techniques, we successfully localized three-dimensional positions of single inhibitory synaptic vesicles loaded with QD-conjugated antibodies against the luminal domain of VGAT. Figure 1C shows the real-time three-dimensional trace of one single QD-loaded inhibitory synaptic vesicle in living neurons with the x-y plane projection overlaid on the fluorescence image of an inhibitory presynaptic terminal with VGAT-CypHer5E-labeled vesicles during 1200 stimuli (10 Hz for 120 s). The trace in Fig. 1C indicates that the single inhibitory synaptic vesicle remained at the edge of a presynaptic terminal, before undergoing exocytosis at 32.0 s. Fluorescence images of the QD-loaded inhibitory synaptic vesicles before and after exocytosis (Fig. 1D) clearly show almost complete quenching of the QD. We further analyzed average fluorescence intensity within the region-of-interest (ROI) and the radial distance from the momentary position to the fusion site ($R = \sqrt{X^2 + Y^2 + Z^2}$) of the single QD-loaded inhibitory synaptic vesicle before exocytosis (Fig. 1E). The fluorescence trace in Fig. 1E included photoblinking events at ~8, ~13 and ~15 s, indicating the presence of a single QD inside a single vesicle. At 32.0 s, the fluorescence signal displayed a sharp drop in brightness caused by the exposure of the vesicle lumen to the quencher-containing external solution, indicating the full-collapse fusion of the single inhibitory synaptic vesicle loaded with a single QD. Thus, the example shown in Fig. 1 demonstrates that a single inhibitory synaptic vesicle was successfully labeled with a QD-conjugated antibodies against the luminal domain of VGAT by external stimuli and this single QD-labeled inhibitory synaptic vesicle was tracked in three dimensions up to the moment of

exocytosis during electrical stimulation.

In order to check whether QD-conjugated antibodies against the luminal domain of Syt1 also label inhibitory synaptic vesicles, we measured the colocalization between VGAT-CypHer5E-labeled inhibitory presynaptic terminals and synaptic vesicles loaded with QD-conjugated antibodies against Syt1. The colocalization percentage between VGAT-CypHer5E and Syt1-labeled vesicles was $12 \pm 1.4 \%$ ($N = 13$ images)(*SI Appendix*, Fig. S1), implying that our previous observed dynamics of these Syt1-labeled synaptic vesicles (24) mainly represented the dynamics of excitatory synaptic vesicles in the dissociated hippocampal neurons.

In order to find relative proportion of inhibitory neurons in dissociated hippocampal cultures, we co-immunostained for MAP2 (a neuron-specific marker) and glutamic acid decarboxylase 67 (GAD67 - a marker for inhibitory neurons) in our hippocampal cultures (Fig. 2A). The colocalization percentage between fluorescence puncta of MAP2 and GAD67 was $6 \pm 0.8 \%$ ($N = 23$ images)(Fig. 2B), which indicates that our dissociated hippocampal cultures are predominantly excitatory neurons. To further find the identity of inhibitory neurons in our hippocampal cultures, we co-immunostained GAD67 and parvalbumin (PV) in fixed primary hippocampal neurons. The colocalization percentage between fluorescence puncta of GAD67 and PV was $82 \pm 7.7 \%$ ($N = 19$ images)(Fig. 2C), indicating that PV-expressing fast-spiking GABAergic interneurons were dominant in our inhibitory neurons in our dissociated hippocampal cultures. Therefore, our VGAT-labeled synaptic vesicles likely represent

the dynamics of inhibitory synaptic vesicles in fast-spiking PV-expressing GABAergic interneuron.

Unique spatiotemporal dynamics of single inhibitory synaptic vesicles

In order to understand the dynamics of exocytosed inhibitory synaptic vesicles, we investigated the net displacements between the initial positions and their fusion sites of single releasing inhibitory synaptic vesicles during electrical stimulation. Three-dimensional net displacement was calculated as Pythagorean displacements using our real-time 3D traces of single QD-loaded inhibitory synaptic vesicles. Figure 3A shows the net displacements of inhibitory synaptic vesicles compared with our previously reported net displacements of Syt1-labeled synaptic vesicles (24). Net displacements between the initial and fusion sites of inhibitory synaptic vesicles were not significantly different from that of Syt1-labeled synaptic vesicles ($p > 0.7$, Kolmogorov–Smirnov (K-S) test) (Fig. 3A).

To further understand the motion of inhibitory vesicles, we calculated the three-dimensional total travel length before fusion of inhibitory synaptic vesicles. The total travel length before fusion of inhibitory synaptic vesicles undergoing exocytosis (average, 10.8 ± 0.94 (standard error of the mean) μm ($n = 80$)) was significantly smaller than that of Syt1-labeled vesicles (18.7 ± 2.32 μm ($n = 49$), $p < 0.05$, K-S test; Fig. 3B). These results indicated that inhibitory synaptic vesicles traveled less to reach fusion sites than excitatory synaptic vesicles since Syt1-labeled vesicles are likely to represent excitatory synaptic vesicles in our cultures. The smaller travel length before

fusion and not significantly different net displacement of inhibitory synaptic vesicles suggest more exocytosis at earlier times compared with excitatory synaptic vesicles.

In order to test that hypothesis, we measured the fusion time between initial stimulation and fusion of inhibitory synaptic vesicles. Figure 3C shows the cumulative fusion time of inhibitory synaptic vesicles compared with that of Syt1-labeled synaptic vesicles. The fusion time of inhibitory synaptic vesicle during stimulation (26.2 ± 2.24 s), was significantly shorter than Syt1-labeled vesicles (44.2 ± 4.89 s) ($p < 0.01$, K-S test). These results indicate that inhibitory synaptic vesicles undergo faster exocytosis than the excitatory synaptic vesicles. We further investigated exocytosis kinetics by calculating the number of fusion events every 20 s. A higher percentage of inhibitory synaptic vesicles underwent exocytosis in the first two 20 s ($31/80 = 38.8\%$ in $t < 20$ s, $35/80 = 43.8\%$ in $20 \leq t < 40$ s) compared with Syt1 labeled vesicles ($16/49 = 32.7\%$ in $t < 20$ s, $10/49 = 20.4\%$ in $20 \leq t < 40$ s), which is consistent with the higher release probability of inhibitory synaptic vesicles compared with excitatory synaptic vesicles (16, 17).

Relation of release probability to position and travel length of inhibitory synaptic vesicles

Whether vesicles' proximity to fusion sites determines their release probability ($P_{r/v}$) is a crucial question in neuroscience. Recent real-time tracking of Syt1-labeled vesicles indicates that vesicles' proximity to fusion sites is a key factor in determining the release probability of Syt1-labeled synaptic vesicles (24). However, the relationship

between the proximity to their fusion sites and the release probability ($P_{r/v}$) of inhibitory synaptic vesicles is unknown. Thus, we answered this question by investigating the relationship between the fusion time and their net displacements. Figure 4A shows that the net displacement of inhibitory synaptic vesicles is related to their fusion time (Pearson's $r = 0.77$), indicating a correlation between the proximity to fusion sites and release probability of inhibitory synaptic vesicles. The slope of inhibitory synaptic vesicles in Fig. 4A (0.079 ± 0.00745 (\pm SEM)) was smaller than that of Syt1-labeled vesicles (0.11346 ± 0.01632)(*SI Appendix*, Fig. S3), indicating the faster exocytosis of inhibitory synaptic vesicles located in the same net displacement. Using net displacement, we calculated net velocity of releasing inhibitory synaptic vesicles. Average net velocity of releasing inhibitory synaptic vesicles was 5.4 ± 0.54 nm/s, which was higher than that of releasing Syt1-labeled vesicles (4.7 ± 0.74 nm/s). The difference was not significant ($p > 0.2$, *K-S test*). The coefficient of variation (CV) in net velocity of inhibitory synaptic vesicles was 89%, which is smaller than that of Syt1-labeled synaptic vesicles (110%). The smaller CV indicates that net speed of inhibitory synaptic vesicles is less variable to reach their fusion sites.

We further investigated the relationship between the total travel length before fusion and fusion time of inhibitory synaptic vesicles. The total travel length before fusion of inhibitory synaptic vesicles is highly related to their fusion time (Pearson's $r = 0.94$)(Fig. 4C), indicating a close correlation between the travel length and release probability of inhibitory synaptic vesicles. This higher value of Pearson correlation coefficient compared with net displacement indicates that fusion time is

more closely related to total travel length before fusion than net displacement of synaptic vesicles. The slope of inhibitory synaptic vesicles (1.43 ± 0.059 (\pm SEM)) was smaller than that of Syt1-labeled vesicles (1.58 ± 0.095), indicating the faster exocytosis of inhibitory synaptic vesicles. Using total travel length before fusion, we calculated speed of releasing inhibitory synaptic vesicles. Speed of releasing inhibitory synaptic vesicles (405 ± 13.9 nm/s) was significantly lower than that of releasing Syt1-labeled vesicles (448 ± 28.1 nm/s). The CV in speed of inhibitory synaptic vesicles (31%) was smaller than that of Syt1-labeled synaptic vesicles (44%), indicating that inhibitory synaptic vesicles undergo more tightly regulated movement. The higher velocity and lower speed before fusion of inhibitory synaptic vesicles imply that inhibitory synaptic vesicles moved to fusion sites more straightly than Syt1-labeled vesicles.

Exocytotic fusion mode of single inhibitory synaptic vesicles

Finally, we investigated the exocytotic fusion mode of single inhibitory synaptic vesicles. Since fusion pore opening is brief in kiss-and-run fusion, trypan blue (quencher) in external solution equilibrate only partially, which give partial quenching compared with full-collapse fusion (24). Figure 5A shows the fluorescence images of a QD inside an inhibitory synaptic vesicle undergoing kiss-and-run fusion, taken before any fluorescence drop (70.2 s), after partial loss of fluorescence (71.2 and 105 s), and after subsequent loss of the remaining fluorescence (105.9 s). A fluorescence trace, obtained by analysis of the region-of-interest (ROI) containing the QD (Fig. 5B), displays a sudden and irreversible decrease in fluorescence (red arrow) at 70.5 s. At

105.2 s, the fluorescence signal dropped further (blue arrow) and settled at a lower level reflecting near-complete quenching, representing full-collapse fusion. The average fluorescence of the QD for the period from 70.5 s to 105.2 s was reduced to 0.35 compared with an initial level, significantly larger than that expected for QDs steadily exposed to 2 μ M TB (0.12). To further confirm that the partial quenching can be used as indicator of kiss-and-run fusion, we divided all fluorescence traces depending on the quenching pattern. We observed three patterns: almost complete quenching (presumably full-collapse fusion), partial quenching followed by almost complete quenching (presumably the first kiss-and-run fusion followed by full-collapse fusion or reuse after the first kiss-and-run fusion), and partial quenching not followed by complete quenching (the first kiss-and-run not followed by full-collapse fusion or no immediate reuse after the first kiss-and-run fusion). Figure 5C shows the average normalized fluorescence intensities with SEM in time aligned with the first fusion depending on the quenching pattern. The average remaining normalized fluorescence right after the full-collapse fusion (Fig. 5C1) was smaller 0.12 whereas the kiss-and-run fusion (Fig. 5C2 and 5C3) was higher than 0.12. This clear difference in the remaining normalized fluorescence after the first fusion depending on fusion mode confirms that the partial quenching is a good indicator of kiss-and-run fusion in our experiments.

Based on the partial quenching as the reporter of kiss-and-run fusion, we also calculated the prevalence of kiss-and-run fusion. We observed ~ 2.5 fold greater prevalence of kiss-and-run fusion in inhibitory synaptic vesicles compared with Syt1-

labeled synaptic vesicles (Fig. 5D), indicating that inhibitory synaptic vesicles undergo kiss-and-run fusion more frequently than excitatory synaptic vesicles. The high prevalence of kiss-and-run fusion of inhibitory synaptic vesicles may make inhibitory synaptic vesicles available for continuous release of neurotransmitter during prolonged stimulation in inhibitory synaptic transmission.

We further investigated the dynamics of inhibitory synaptic vesicles based on fusion modes and compared them with Syt1-labeled vesicles. The total travel length of inhibitory synaptic vesicles undergoing full-collapse fusion (16.9 ± 1.66 (n = 28) μm) was larger than that of Syt1-labeled vesicles (30.6 ± 3.09 (n = 36) μm , $p < 0.05$, K-S test)(Fig. 5E). Total travel length of inhibitory synaptic vesicles undergoing kiss-and-run fusion (20.4 ± 1.48 (n = 52) μm) was similar to that of Syt1-labeled vesicles (21.0 ± 3.09 s (n = 13) μm , $p > 0.7$, K-S test)(Fig. 5F). The fusion time of inhibitory synaptic vesicles undergoing full-collapse fusion was significantly shorter than that of Syt1-labeled vesicles undergoing full-collapse fusion (20.3 ± 3.03 s (n = 28) vs. 44.7 ± 5.84 s (n = 36), respectively; ($p < 0.01$, K-S test)) (Fig. 5G). Fusion times of inhibitory synaptic vesicles undergoing kiss-and-run fusion were not significantly different from those of Syt1-labeled synaptic vesicles undergoing kiss-and-run fusion ($p > 0.4$, K-S test) (Fig. 5H). These results indicate that the observed unique dynamics of inhibitory synaptic vesicles is mainly caused by the difference in the dynamics of inhibitory synaptic vesicles undergoing full-collapse fusion (significantly shorter travel length and faster fusion time).

Discussion

The structures and functions of GABAergic inhibitory synapses are different from those of glutamatergic excitatory synapses. GABAergic inhibitory neurons are crucial in controlling the number and activity level of glutamatergic excitatory neurons and firing frequency via fast feedforward and feedback inhibition in neuronal networks (17, 30, 31). To allow for fast synaptic transmission without synaptic failure, inhibitory neurons adopt a distinct set of morphology, multiple release sites, biogenesis and trafficking processes for synaptic vesicles in presynaptic terminals (20, 32-34). In particular, Ca^{2+} channels are tightly coupled to the GABA release molecular machinery, to increase the speed and efficacy of GABA transmission, which in turn provides a relatively higher energy efficiency of vesicle release in the presynaptic terminals of inhibitory neurons (35). Although the higher release probability and reliability of action potential-evoked Ca^{2+} signal play an important role in the GABA release mechanisms to maintain timely synaptic transmission, the actual exocytosis and dynamics of single synaptic vesicles throughout the processes of vesicle release and recycling in GABAergic inhibitory presynaptic terminals has been unknown.

In this study, we loaded single inhibitory synaptic vesicles with QDs-conjugated antibodies against the luminal domain of VGAT in hippocampal neurons and tracked single inhibitory synaptic vesicles in three dimensions up to the moment of exocytosis. To compare dynamics of inhibitory vesicles with that of glutamatergic excitatory synaptic vesicles, we used synaptic vesicles labeled with QD-conjugated antibodies against the luminal domain of Syt1 for excitatory synaptic vesicles in cultured

hippocampal neurons because the great majority of neurons in our hippocampal cultures are excitatory (Fig. 2) and Syt1-labeled synaptic vesicles mainly label excitatory synaptic vesicles (SI Appendix Fig. 1). Although around 10 % of Syt1-labeled synaptic vesicles were colocalized with VGAT-CypHer5E-labeled presynaptic terminals and Syt1 plays a key role as a Ca^{2+} sensor in both glutamatergic and GABAergic presynaptic terminals (36), our previous results obtained from Syt1-labelled synaptic vesicles in cultured hippocampal neurons mainly represent the properties of excitatory synaptic vesicles (24). Interestingly, the fast synchronous vesicle release was abolished in glutamatergic presynaptic terminals (granule cell-basket cell synapse) but not GABAergic presynaptic terminals (basket cells-granule cells synapse) in the hippocampus of Syt1 KO mice (37). In addition, a subset of PV-expressing hippocampal interneurons mainly use Syt2 as the main Ca^{2+} sensor (38) and GABAergic inhibitory neurons have an alternative high-affinity Ca^{2+} sensor, DOC2 β , to control spontaneous release (36, 38). Even though more than 21 types of interneurons are localized in the hippocampus, our immunostaining results showed that less than 10% of the cultured hippocampal neurons are inhibitory neurons and ~80% of those inhibitory neurons were PV)-expressing interneurons. Given these pieces of evidence, our previous results obtained from Syt1-labelled synaptic vesicles in cultured hippocampal neurons likely represent the properties of excitatory synaptic vesicles (24).

Here, we found that the total travel length before exocytosis of inhibitory synaptic vesicles were smaller than those of Syt1-labelled synaptic vesicles. Intriguingly, inhibitory synaptic vesicles underwent exocytosis earlier than those of Syt1-labeled

vesicles and a larger portion of the inhibitory synaptic vesicles was released within 40 s of the onset of stimulation. Release probability of inhibitory synaptic vesicles was closely related to the proximity to fusion sites and total travel length. These results indicate that inhibitory synaptic vesicles move to their fusion sites more directly than Syt1-labeled synaptic vesicles. Inhibitory synaptic vesicles also exhibited a higher prevalence of kiss-and-run fusion. The smaller travel length before exocytosis, shorter fusion time, and a higher prevalence of kiss-and-run fusion of inhibitory synaptic vesicles represent the unique dynamics and exocytosis of inhibitory synaptic vesicles, which is consistent with previously reported electrophysiological and ultrastructural features of inhibitory synaptic transmission—a larger RRP size, fast short-term depression and higher release probability in inhibitory synaptic vesicles (16, 17). Furthermore, these observed dynamics suggests efficient and fast neurotransmitter release of inhibitory neurons in our primary hippocampal neurons - mainly PV-expressing interneurons. This fast and efficient release of inhibitory synaptic vesicles enables PV-expressing interneurons to signal rapidly, which makes possible higher microcircuit functions in the brain including feedforward and feedback inhibition and high-frequency network oscillations on fast timescales (40). The differences in vesicle dynamics between inhibitory and excitatory synaptic vesicles suggest that the distinct dynamics of synaptic vesicles affect the synaptic functions, despite the overlapping molecular machinery of synaptic release. In line with the importance of localization and movement of synaptic vesicles, the altered relationship between the release probability and position of synaptic vesicles can affect the release of neurotransmitters in

neurodegenerative diseases, such as Huntington's disease (41, 42).

The unique dynamics of single inhibitory synaptic vesicles can contribute to fast inhibitory synaptic transmission and fast short-term depression. The shorter travel length before exocytosis and proximity of inhibitory synaptic vesicles with high release probability ($P_{r/v}$) to fusion sites enable inhibitory synaptic vesicles to undergo exocytosis earlier than excitatory synaptic vesicles, observed as significantly shorter fusion time of inhibitory synaptic vesicles (Fig. 3). The shorter fusion time will contribute to the faster inhibitory synaptic transmission upon the stimulation. In addition to unique dynamics of inhibitory synaptic vesicles, other mechanisms can also contribute to fast inhibitory synaptic transmission.

The specific mechanism driving the unique dynamics of single inhibitory synaptic vesicles compared to excitatory synaptic vesicles is not known. However, the underlying principles can be deduced from the distinct molecular and structural profiles of the inhibitory presynaptic terminals, which influence the encoding of signals via fast and efficient synaptic transmission. The distinct types of Ca^{2+} channels, larger RRP size, higher release probability and tight coupling between the Ca^{2+} channels and Ca^{2+} sensor have been thought to support fast inhibitory synaptic transmission and prevent synaptic fatigue in the inhibitory presynaptic terminals.

In summary, we showed that inhibitory synaptic vesicles travel less to reach their fusion sites before exocytosis. We also found that inhibitory synaptic vesicles undergo faster exocytosis and exhibit a higher prevalence of kiss-and-run fusion. This unique dynamics and exocytosis of inhibitory synaptic vesicles can be a novel process to

mediate the precise conversion of input signals into output signals in hippocampal inhibitory neurons. Thus, our data suggest that unique dynamics and exocytosis of inhibitory synaptic vesicles is one of important factors in inhibitory synaptic transmission.

Materials and methods

Primary hippocampal neuron culture.

Rat (Sprague Dawley) pups at the postnatal 0-day (P0) were sacrificed to harvest CA1 and CA3 of the hippocampal regions of the brain tissue as previously described(24, 43). All procedures were performed according to the animal protocol approved by the Department of Health, Government of Hong Kong. Around 2×10^4 neurons were plated on each Poly D-Lysine (P7886, Sigma-Aldrich, USA)-coated cover glass with a diameter of 12 mm (Glaswarenfabrik Karl Hecht GmbH & Co KG, Germany) in 24-well plates. Two days after plating the neurons, 10 μ M uridine (U3003, Sigma-Aldrich) and 10 μ M 5-fluorodeoxyuridine (F0503, Sigma-Aldrich) were added to inhibit the proliferation of glial cells in cultured neurons(44). The neurons were cultured in the NeurobasalTM-A Medium (10888022, Thermo Fisher Scientific, USA) supplemented with 2.5 % FBS, 1 % Penicillin-Streptomycin (15140122, Thermo Fisher Scientific), 500 μ M GlutaMAXTM-I Supplement (A1286001, Thermo Fisher Scientific), and 2 % B-27TM Supplement (17504001, Thermo Fisher Scientific). Cultured neurons were maintained in a 5% CO₂ incubator at 37°C before experiments were performed.

Microscopy setup.

463 A real-time three-dimensional tracking microscope with a custom-built dual-focus
 464 imaging optics was built as previously described (24). The dual-focus imaging optics
 465 was made up of an aperture, a beam splitter, lenses, mirrors and a right angle mirror. In
 466 the dual-focus imaging optics, the beam splitter divided fluorescent signals into two
 467 beam pathways, the focus plane of each beam pathway was determined by its lens, and
 468 two fluorescence signals from each beam pathway were imaged side-by-side in an
 469 electron multiplying (EM) CCD camera. An Olympus IX-73 inverted fluorescence
 470 microscope (Olympus, Japan) equipped with an EMCCD camera (iXon Ultra, Andor,
 471 UK) was used to acquire fluorescence signals as previously described (45). An oil
 472 immersion 100x objective with NA = 1.40 (UPlanSApo, Olympus) was used for
 473 imaging Streptavidin-coated quantum dots (QD 625, A10196, Life Technologies)-
 474 conjugated antibodies against VGAT and CypHer5E-conjugated antibodies against
 475 VGAT. In order to locate two-dimensional centroids and to calculate the fluorescent
 476 peak intensity at different focal planes (I_1 and I_2), we used custom-written IDL coded
 477 programs (L3Harris Geospatial, USA) to fit a two-dimensional Gaussian function to
 478 the fluorescence image. An objective scanner (P-725.2CD, Physik Instrumente (PI),
 479 Germany) was used to generate a calibration curve based on the z-position dependence
 480 of the normalized intensity difference ($(I_1 - I_2)/(I_1 + I_2)$). Custom-made programs written
 481 in LabVIEW (National Instruments, USA) were used to control an objective scanner
 482 and acquire data on the z-position. The z-positions of quantum dots (QDs) were
 483 obtained from the relative peak intensity differences using the empirically determined
 484 calibration curve, as previously described (24, 28). A 405 nm laser (OBIS, Coherent

Inc., USA) and a 640 nm laser (OBIS, Coherent Inc.) were used to illuminate streptavidin coated QDs and CypHer5E, respectively. A 15× beam expander (Edmund Optics) and a focus lens (Newport Corporation, USA) were used to illuminate the sample uniformly.

Real-time imaging of single inhibitory synaptic vesicles.

Imaging experiments were performed using 14 - 21 days in vitro (DIV) rat primary hippocampal neurons at room temperature. Neurons were pre-incubated with 3 nM of CypHer5E-tagged anti-VGAT antibodies (131 103CpH, Synaptic Systems, Germany) in the culture medium and incubated in the 5% CO₂ incubator for 2 h at 37°C to specifically label inhibitory synaptic vesicles in presynaptic terminals. Then, single inhibitory synaptic vesicles were labeled by QDs conjugated with antibodies against the luminal domain of VGAT. To conjugate QDs to antibodies, Streptavidin-coated quantum dots 625 (A10196, Thermo Fisher Scientific) were incubated with biotinylated antibodies against the luminal domain of VGAT (131 103BT, Synaptic Systems) in a modified Tyrode's solution (4 mM KCl, 150 mM NaCl, 2 mM CaCl₂, 2 mM MgCl₂, 10 mM D-glucose, 10 mM HEPES, 310-315 mOsm/kg, and pH 7.3-7.4) with casein (C7078, Sigma-Aldrich) for 50 min at room temperature. After the incubation, the conjugated solution was added to a sample chamber containing a cover glass with neurons dipped in the modified Tyrode's solution. The labeling of single inhibitory synaptic vesicles with QDs was conducted by triggering evoked release of synaptic vesicles using 10 Hz electric field stimulation for 120 s, which was induced by parallel

platinum electrodes connected with the SD9 Grass stimulator (Grass Instruments, USA).

Following 2 min incubation after stimulation, the Tyrode's solution was superfused for

15 min at 1.0 ~ 2.0 ml/min. Subsequently, 2 μ M of trypan blue (15250061, Thermo

Fisher Scientific) were superfused before imaging. During the imaging, trypan blue

(quencher) were kept in the chamber to quench the fluorescence of QDs exposed to

external solution during exocytosis. Fluorescence images of CypHer5E-labeled and

QD-labeled synaptic vesicles were acquired using an Olympus IX-73 inverted

microscope. A ZT640rdc-UF1 (Chroma Technology, USA) and an ET690/50M

(Chroma Technology) were used to acquire fluorescence images of CypHer5E-labeled

presynaptic boutons. A ZT405rdc-UF1 (Chroma Technology) and an ET605/70M

(Chroma Technology) were used to acquire fluorescence images of QD-labeled

inhibitory synaptic vesicles. 2000 frame images were obtained using a frame-transfer

mode at 10 Hz for 200 s using an EMCCD camera. The EMCCD camera and the

stimulator were synchronized with Axon Digidata 1550 (Molecular Devices, USA) to

trigger an electric field stimulation at 10 Hz for 120 s while recording. Clampex

(program, Molecular Devices) was used to generate stimulation protocols and control

stimulation based on the protocol.

Analysis of the real-time single vesicle-tracking images.

Custom-written IDL coded programs were used to localize the centroids of raw

fluorescence images. Two-dimensional centroids and peak intensities of synaptic

vesicles loaded with QDs at two different focal planes were calculated by fitting a

Gaussian function to fluorescence images using custom-written programs using IDL.

The position along the z-axis was calculated based on a calibration curve while the average intensity of the fluorescence of a QD within a region of interest (ROI) was calculated using MetaMorph (Molecular Devices). Fusion positions and times of single synaptic vesicles were determined as the first quenching positions and times of fluorescence intensity by trypan blue during electrical stimulation similar to the previous report (24). Two-sample Kolmogorov-Smirnov tests (K-S test) were used for statistical analysis, using OriginPro 9.1 (OriginLab, USA). Data are presented as the mean \pm standard error of the mean (SEM). Differences with $p < 0.05$ was considered significant.

Immunofluorescence.

For immunocytochemistry, neurons at DIV14 were washed with PBS once, then fixed with ice-cold 100% methanol for 10 minutes at -20°C. After three washes in PBS for 30 min at room temperature, cells were incubated with Chicken antibody against MAP2 (1:1000, ab5392, Abcam), Rabbit antibody against Parvalbumin (1:500, PA1-933, Thermo Fischer Scientific) and Mouse antibody against GAD67 (1:500, MAB5406, Sigma-Aldrich) in staining buffer (0.2% BSA, 0.8 M NaCl, 0.5% Triton X-100, 30 mM phosphate buffer, pH 7.4) overnight at 4°C. Neurons were then washed three times in PBS for 30 min at room temperature and incubated with Alexa Fluor conjugated secondary antibodies (Goat anti-Chicken-Alexa 488, A11039, Life Technologies; Goat anti-Rabbit-Alexa 568, A11011, and Donkey anti-Mouse-Alexa 647, A31571, Life Technologies) with 1:1000 dilution in staining buffer for 2 hours at room temperature

and stained with DAPI (300 nM, D1306, Thermo Fisher Scientific) for 10 minutes at room temperature. After washed three times in PBS for 30 min, Cover glasses were mounted onto microscope slides with HydroMount medium (National Diagnostics). Confocal images were acquired using a SP8 confocal microscope (Leica) with a 40x oil objective.

Quantification of colocalization.

Biotinylated mouse monoclonal antibody against the luminal domain of vesicular protein Syt1 (105 311BT, Synaptic System) were conjugated with QD 625 streptavidin-conjugates (A10196, Thermo Fisher Scientific) in order to label single SVs. The conjugation and labeling methods are the same as the previously described methods for VGAT-QDs. VGAT-CypHer5E (131 103CpH, Synaptic System) were used to label inhibitory presynaptic terminals by the incubation for 3 hours after experiments. Syt1-labeled SVs localized in inhibitory presynaptic boutons were counted, based on the colocalization of the fluorescence signals of QDs and CypHer5E.

Supporting Information

This article contains supporting information online at

Acknowledgements

We thank Ching Yeung Fan, Cheuk Long Frank, Lee, Keun Yang Park for help with data analyses and members of Park lab for helpful discussion and comments. We also

thank Chenglu Tao for discussion. We thank Dr. Curtis Barrett for critically reading the manuscript and for providing constructive comments. This work was supported by the Research Grants Council of Hong Kong (Grants 26101117, 16101518, A-HKUST603/17 and N_HKUST613/17) and the Innovation and Technology Commission (ITCPD/17-9).

Declaration of interests

The authors declare no conflict of interest.

REFERENCES

1. T. C. Sudhof, Calcium control of neurotransmitter release. *Cold Spring Harbor perspectives in biology* **4**, a011353 (2012).
2. C. Yu, M. Zhang, X. Qin, X. Yang, H. Park, Real-time imaging of single synaptic vesicles in live neurons. *Frontiers in Biology* **11**, 109-118 (2016).
3. V. N. Murthy, P. D. Camilli, CELL BIOLOGY OF THE PRESYNAPTIC TERMINAL. *Annu. Rev. Neurosci* **26**, 701-728 (2003).
4. T. C. Sudhof, Neurotransmitter release: the last millisecond in the life of a synaptic vesicle. *Neuron* **80**, 675-690 (2013).
5. A. Malgaroli, R. W. Tsien, Glutamate-induced long-term potentiation of the frequency of miniature synaptic currents in cultured hippocampal neurons. *Nature* **357**, 134-139 (1992).
6. S. Kim *et al.*, Loss of IQSEC3 Disrupts GABAergic Synapse Maintenance and Decreases Somatostatin Expression in the Hippocampus. *Cell reports* **30**, 1995-2005.e1995 (2020).
7. T. Klausberger, P. Somogyi, Neuronal diversity and temporal dynamics: the unity of hippocampal circuit operations. *Science (New York, N.Y.)* **321**, 53-57 (2008).
8. S. F. Owen *et al.*, Oxytocin enhances hippocampal spike transmission by modulating fast-spiking interneurons. *Nature* **500**, 458-462 (2013).
9. H. L. Atwood, S. Karunanithi, Diversification of synaptic strength: presynaptic elements. *Nature reviews. Neuroscience* **3**, 497-516 (2002).
10. P. S. Kaeser, W. G. Regehr, The readily releasable pool of synaptic vesicles. *Current opinion in neurobiology* **43**, 63-70 (2017).
11. M. Kneussel, T. J. Hausrat, Postsynaptic Neurotransmitter Receptor Reserve Pools for Synaptic Potentiation. *Trends in neurosciences* **39**, 170-182 (2016).
12. M. Yoshihara, J. T. Littleton, Synaptotagmin I functions as a calcium sensor to synchronize neurotransmitter release. *Neuron* **36**, 897-908 (2002).
13. O. D. Bello *et al.*, Synaptotagmin oligomerization is essential for calcium control of regulated exocytosis. *Proceedings of the National Academy of Sciences of the United States of America* **115**, E7624-e7631 (2018).
14. K. Grushin *et al.*, Structural basis for the clamping and Ca(2+) activation of SNARE-mediated fusion by synaptotagmin. *Nature communications* **10**, 2413 (2019).
15. G. Voglis, N. Tavernarakis, The role of synaptic ion channels in synaptic plasticity. *EMBO reports* **7**, 1104-1110 (2006).
16. R. Nair *et al.*, Neurobeachin regulates neurotransmitter receptor trafficking to synapses. *The Journal of cell biology* **200**, 61-80 (2013).
17. U. Kraushaar, P. Jonas, Efficacy and stability of quantal GABA release at a hippocampal interneuron-principal neuron synapse. *The Journal of neuroscience : the official journal of the Society for Neuroscience* **20**, 5594-5607 (2000).
18. K. Jensen, J. D. Lambert, M. S. Jensen, Activity-dependent depression of GABAergic IPSCs in cultured hippocampal neurons. *Journal of neurophysiology* **82**, 42-49 (1999).
19. S. Hefft, U. Kraushaar, J. R. Geiger, P. Jonas, Presynaptic short-term depression is maintained during regulation of transmitter release at a GABAergic synapse in rat hippocampus. *The Journal of physiology* **539**, 201-208 (2002).
20. D. Gitler *et al.*, Different presynaptic roles of synapsins at excitatory and inhibitory synapses.

- 625 *The Journal of neuroscience : the official journal of the Society for Neuroscience* **24**, 11368-
626 11380 (2004).
- 627 21. J. Feng *et al.*, Regulation of neurotransmitter release by synapsin III. *The Journal of*
628 *neuroscience : the official journal of the Society for Neuroscience* **22**, 4372-4380 (2002).
- 629 22. Y. Humeau *et al.*, Synapsin controls both reserve and releasable synaptic vesicle pools during
630 neuronal activity and short-term plasticity in Aplysia. *The Journal of neuroscience : the official*
631 *journal of the Society for Neuroscience* **21**, 4195-4206 (2001).
- 632 23. S. Terada, T. Tsujimoto, Y. Takei, T. Takahashi, N. Hirokawa, Impairment of inhibitory synaptic
633 transmission in mice lacking synapsin I. *The Journal of cell biology* **145**, 1039-1048 (1999).
- 634 24. H. Park, Y. Li, R. W. Tsien, Influence of synaptic vesicle position on release probability and
635 exocytotic fusion mode. *Science (New York, N.Y.)* **335**, 1362-1366 (2012).
- 636 25. Y. Hua *et al.*, A readily retrievable pool of synaptic vesicles. *Nat. Neurosci.* **14**, 833-839 (2011).
- 637 26. H. Park, E. Toprak, P. R. Selvin, Single-molecule fluorescence to study molecular motors.
638 *Quarterly reviews of biophysics* **40**, 87-111 (2007).
- 639 27. A. Yildiz, P. R. Selvin, Fluorescence imaging with one nanometer accuracy: application to
640 molecular motors. *Acc Chem Res* **38**, 574-582 (2005).
- 641 28. T. M. Watanabe, T. Sato, K. Gonda, H. Higuchi, Three-dimensional nanometry of vesicle
642 transport in living cells using dual-focus imaging optics. *Biochemical and biophysical research*
643 *communications* **359**, 1-7 (2007).
- 644 29. T. Schikorski, Readily releasable vesicles recycle at the active zone of hippocampal synapses.
645 *Proceedings of the National Academy of Sciences of the United States of America* **111**, 5415-
646 5420 (2014).
- 647 30. Y. Chagnac-Amitai, B. W. Connors, Horizontal spread of synchronized activity in neocortex and
648 its control by GABA-mediated inhibition. *Journal of neurophysiology* **61**, 747-758 (1989).
- 649 31. F. Manseau *et al.*, Desynchronization of neocortical networks by asynchronous release of GABA
650 at autaptic and synaptic contacts from fast-spiking interneurons. *PLoS Biology* **8** (2010).
- 651 32. B. High, A. A. Cole, X. Chen, T. S. Reese, Electron microscopic tomography reveals discrete
652 transcleft elements at excitatory and inhibitory synapses. *Frontiers in synaptic neuroscience* **7**,
653 9 (2015).
- 654 33. C. L. Tao *et al.*, Differentiation and Characterization of Excitatory and Inhibitory Synapses by
655 Cryo-electron Tomography and Correlative Microscopy. *The Journal of neuroscience : the*
656 *official journal of the Society for Neuroscience* **38**, 1493-1510 (2018).
- 657 34. X. Li *et al.*, Presynaptic Endosomal Cathepsin D Regulates the Biogenesis of GABAergic Synaptic
658 Vesicles. *Cell reports* **28**, 1015-1028.e1015 (2019).
- 659 35. C. Williams *et al.*, Coactivation of multiple tightly coupled calcium channels triggers
660 spontaneous release of GABA. *Nature neuroscience* **15**, 1195-1197 (2012).
- 661 36. N. A. Courtney, J. S. Briguglio, M. M. Bradberry, C. Greer, E. R. Chapman, Excitatory and
662 Inhibitory Neurons Utilize Different Ca(2+) Sensors and Sources to Regulate Spontaneous
663 Release. *Neuron* **98**, 977-991.e975 (2018).
- 664 37. A. M. Kerr, E. Reisinger, P. Jonas, Differential dependence of phasic transmitter release on
665 synaptotagmin 1 at GABAergic and glutamatergic hippocampal synapses. *Proceedings of the*
666 *National Academy of Sciences of the United States of America* **105**, 15581-15586 (2008).
- 667 38. B. Bouhours, E. Gjoni, O. Kochubey, R. Schneggenburger, Synaptotagmin2 (Syt2) Drives Fast
668 Release Redundantly with Syt1 at the Output Synapses of Parvalbumin-Expressing Inhibitory

669 Neurons. *The Journal of neuroscience : the official journal of the Society for Neuroscience* **37**,
670 4604-4617 (2017).

671 39. K. A. Pelkey *et al.*, Hippocampal GABAergic Inhibitory Interneurons. *Physiological reviews* **97**,
672 1619-1747 (2017).

673 40. H. Hu, F. C. Roth, D. Vandael, P. Jonas, Complementary Tuning of Na(+) and K(+) Channel Gating
674 Underlies Fast and Energy-Efficient Action Potentials in GABAergic Interneuron Axons. *Neuron*
675 **98**, 156-165.e156 (2018).

676 41. S. Chen, C. Park, X. Qin, H. Park, Altered Single Synaptic Vesicles Dynamics in neurons of
677 Huntington's Disease. (In Submission).

678 42. S. Chen *et al.*, Altered Synaptic Vesicle Release and Ca(2+) Influx at Single Presynaptic Terminals
679 of Cortical Neurons in a Knock-in Mouse Model of Huntington's Disease. *Frontiers in molecular*
680 *neuroscience* **11**, 478 (2018).

681 43. G. Liu, R. W. Tsien, Synaptic transmission at single visualized hippocampal boutons.
682 *Neuropharmacology* **34**, 1407-1421 (1995).

683 44. S. Leow-Dyke *et al.*, Neuronal toll-like receptor 4 signaling induces brain endothelial activation
684 and neutrophil transmigration in vitro. *J Neuroinflamm* **9**, 230 (2012).

685 45. A. Alsina *et al.*, Real-time subpixel-accuracy tracking of single mitochondria in neurons reveals
686 heterogeneous mitochondrial motion. *Biochemical and biophysical research communications*
687 **493**, 776-782 (2017).

688

FIGURE LEGENDS

Fig. 1. Real-time three-dimensional tracking of a single inhibitory synaptic vesicle. (A) Schematic diagram of a streptavidin-conjugated quantum dot (QD) conjugated with biotinylated antibodies against the luminal domain of VGAT by the streptavidin-biotin interaction. (B) Colocalization of single inhibitory synaptic vesicles loaded with QDs (VGAT-QD; green) and CypHer5E-labeled inhibitory presynaptic boutons (VGAT-CypHer5E; red). Scale bar: 1 μ m. (C) Three-dimensional trajectory of an inhibitory synaptic vesicle loaded with a QD laid on the x-y plane of a CypHer5E-labeled presynaptic bouton. A color bar represents elapsed time. This inhibitory synaptic vesicle underwent exocytosis at 32.0 s. (D) Fluorescence images of a VGAT-QD shown in Fig 1C taken before exocytosis (20 s and 31.9 s) and after exocytosis (32.3 s). Scale bar: 0.5 μ m. (E) Three-dimensional trajectory, radial distance from the momentary position to the fusion site ($R = \sqrt{\Delta X^2 + \Delta Y^2 + \Delta Z^2}$), and fluorescence intensity trace of the synaptic vesicle with a QD up to the moment of exocytosis shown in Fig. 1C. Photoblinking events at 8 s, 13 s and 15 s, indicate the presence of a QD inside a synaptic vesicle. Quenching (irreversible loss of fluorescence) at 32.0 s indicates exocytosis of the synaptic vesicle loaded with a QD. Stimulation (10 Hz, 120 s) started at 20 s.

Fig. 2. Inhibitory neurons in primary hippocampal cultures. (A) Representative confocal images of co-immunostained cultured hippocampal neurons with MAP2 (a neuron-specific marker; green), glutamic acid decarboxylase 67 (GAD67; an

inhibitory neuronal marker; red) and parvalbumin (PV; a marker for PV-expressing interneuron; yellow). Nuclei were counterstained with DAPI (blue). Scale bar: 1 μ m. (B) Percentage of GAD67 expressing neurons in MAP2-expressing hippocampal neurons. (C) The percentage of PV-expressing interneurons in GAD67 positive hippocampal neurons.

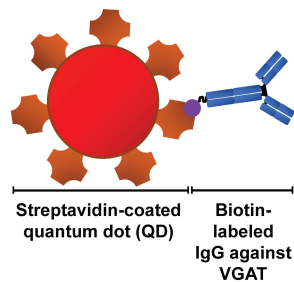
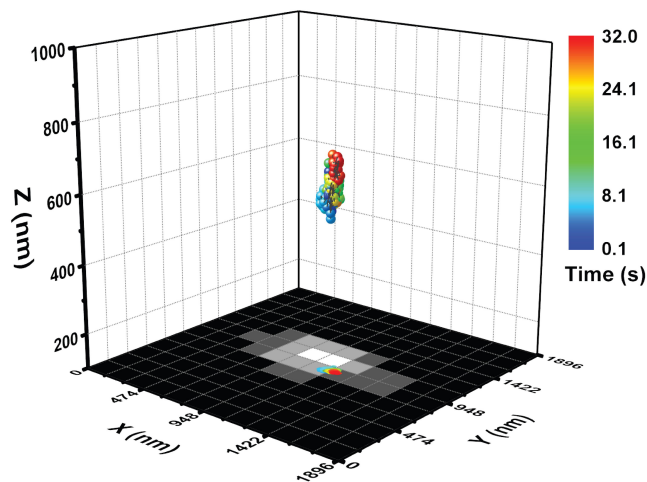
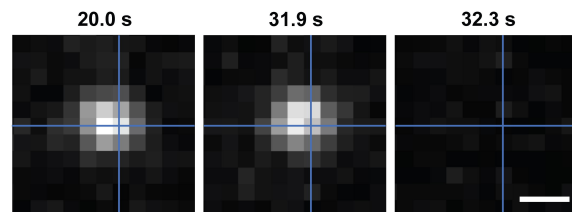
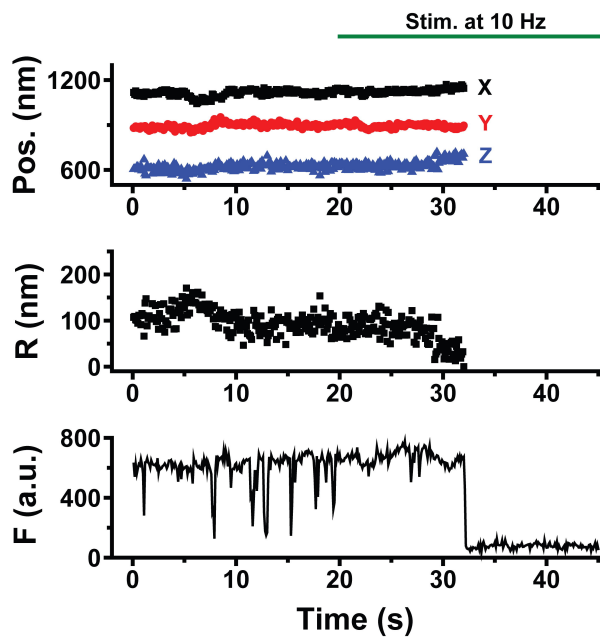
Fig. 3. Distinct spatiotemporal dynamics of single inhibitory synaptic vesicles before exocytosis. (A) Net displacement between initial and fusion sites of VGAT-labeled synaptic vesicles (VGAT SVs, n = 80) and Syt1-labeled synaptic vesicles (Syt1 SVs, n = 49). (B) Total travel length before exocytosis of VGAT-labeled synaptic vesicles. Total travel length of VGAT-labeled synaptic vesicles was significantly smaller than that of Syt1-labeled synaptic vesicles. (C) Fusion time of VGAT-labeled synaptic vesicles and Syt1-labeled synaptic vesicles. Fusion time of VGAT-labeled synaptic vesicles was significantly shorter than that of Syt1-labeled synaptic vesicles. $**p < 0.01$, $*p < 0.05$ and NS, not significant (K-S test).

Fig. 4. Relation of fusion time to net displacement and travel length of inhibitory synaptic vesicles. (A) Relationship between fusion time and net displacement of inhibitory synaptic vesicles. Each dot represents inhibitory synaptic vesicles, and a solid red line represents the linear regression line (Pearson's $r = 0.77$), indicating close relationship between release probability and position of inhibitory synaptic vesicles. (B) Cumulative fraction of net velocity. Net velocity of inhibitory synaptic vesicle was not

significantly different from Syt1-labeled synaptic vesicles. **(C)** Relationship between fusion time and total travel length for inhibitory synaptic vesicles. A larger value of Pearson's correlation (Pearson's $r = 0.94$), indicating strong linear association between release probability and total travel length of inhibitory synaptic vesicles. **(D)** Cumulative fraction of speed. Speed of inhibitory synaptic vesicle was significantly different from Syt1-labeled synaptic vesicles. $**p < 0.01$ and NS, not significant (K-S test).

Fig. 5. Exocytotic fusion mode of inhibitory synaptic vesicles. **(A)** Images before any fluorescence drop (70.2 s), after partial loss of fluorescence (71.2 s), before (105 s), and after subsequent loss of the remaining fluorescence (105.9 s). Scale bar, 0.8 μm . **(B)** 3D position and fluorescence of a QD-loaded vesicle that undergoes kiss-and-run fusion. The unquenched fraction with partial quenching (0.35) was larger than expected unquenched value (0.12). This partial quenching indicates kiss-and-run fusion. A red arrow marks the time of kiss-and-run fusion, and a blue arrow marks the time of full-collapse fusion. Green bar, 10 Hz stimulation for 120 s. **(C)** Average normalized fluorescence intensities with SEM in time aligned with the first fusion depending on three quenching patterns - almost complete quenching (C1), partial quenching followed by almost complete quenching (C2), and partial quenching not followed by complete quenching (C3). The horizontal dot line represents the normalized remaining fluorescence intensity of 0.12 (the expected normalized fluorescence right after full-collapse fusion). **(D)** Prevalence of kiss-and-run fusion. The prevalence of kiss-and-run

fusion in inhibitory synaptic vesicles (65%) was higher than that in Syt1-labeled synaptic vesicles (27%). **(D)** Total travel length of inhibitory synaptic vesicles undergoing full-collapse fusion (VGAT FCF) was significantly different from that of Syt1-labeled synaptic vesicles (Syt1 FCF). **(E)** Total travel length of inhibitory synaptic vesicles undergoing kiss-and-run fusion (VGAT K&R) was not significantly different from that of Syt1-labeled synaptic vesicles (Syt1 K&R). **(F)** Fusion time of inhibitory synaptic vesicles undergoing full-collapse fusion (VGAT FCF) was not significantly different that of Syt1-labeled synaptic vesicles (Syt1 FCF) **(G)** Fusion time of inhibitory synaptic vesicles undergoing kiss-and-run fusion (VGAT K&R) was not significantly different that of Syt1-labeled synaptic vesicles (Syt1 K&R). $*p<0.01$, $**p<0.01$, and NS, not significant (K-S test).

A**B****C****D****E**

A

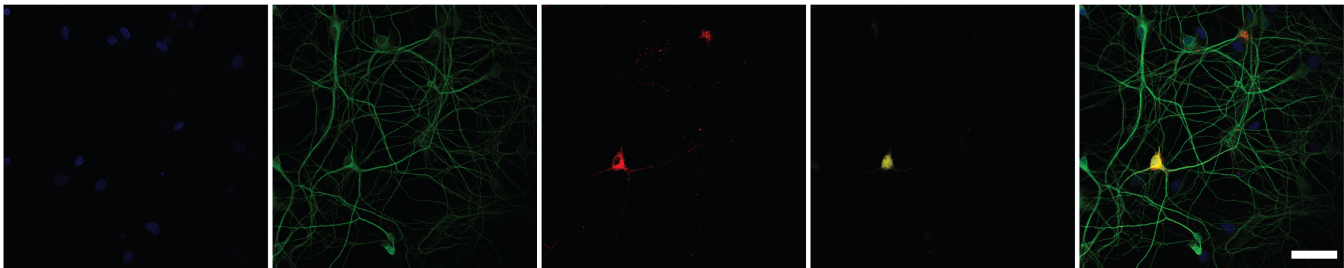
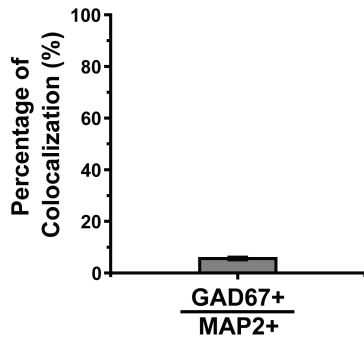
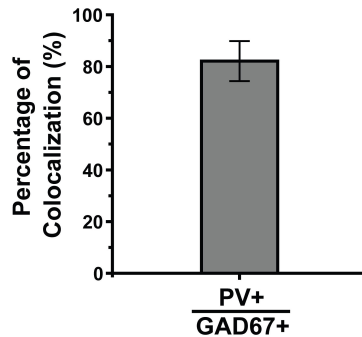
DAPI

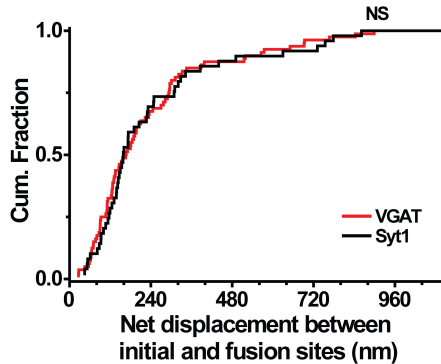
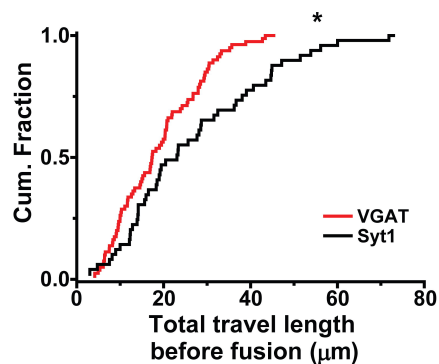
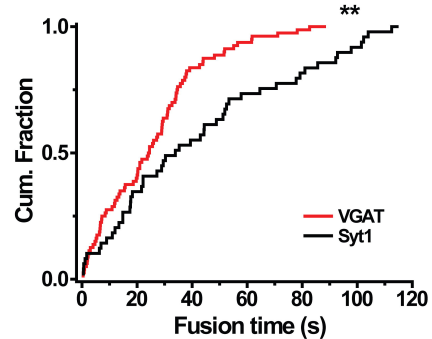
MAP2

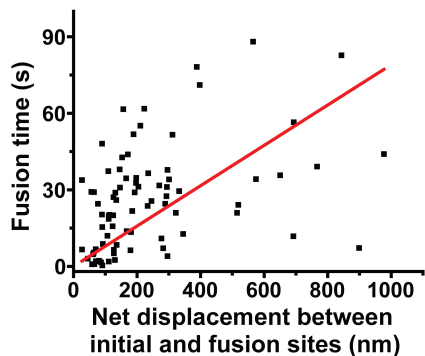
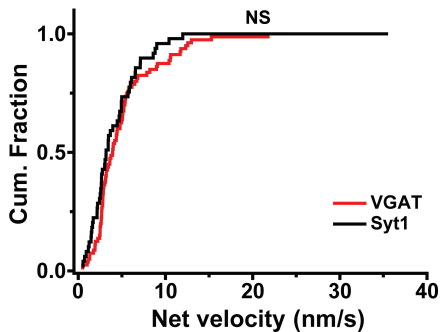
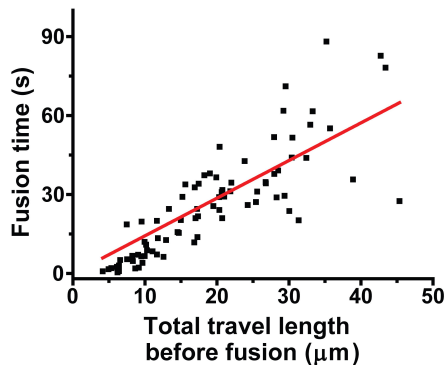
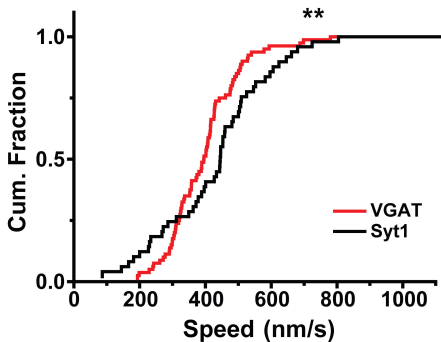
GAD67

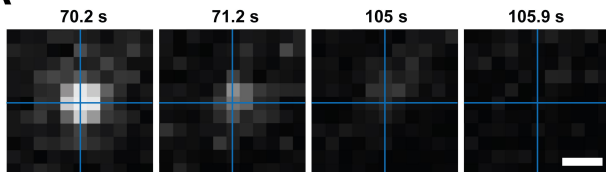
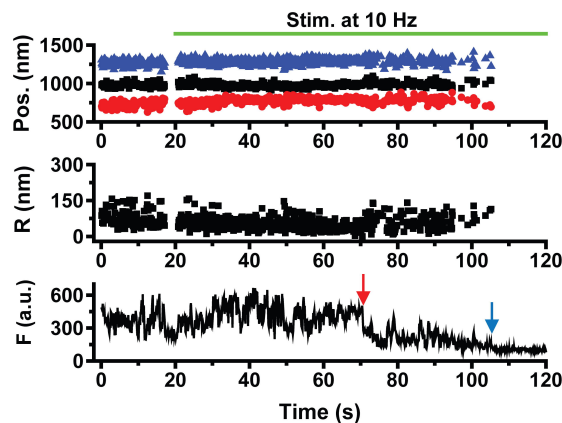
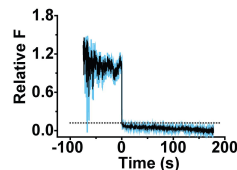
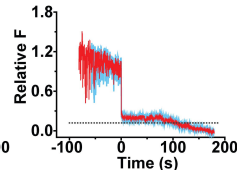
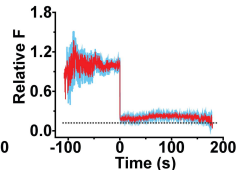
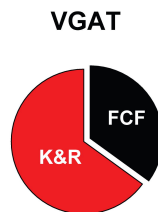
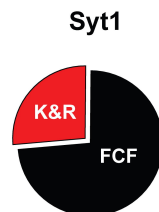
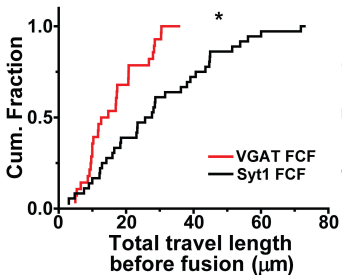
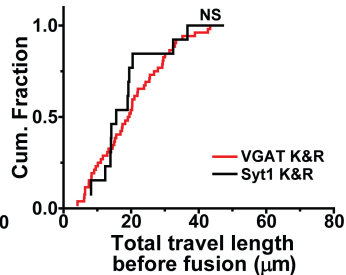
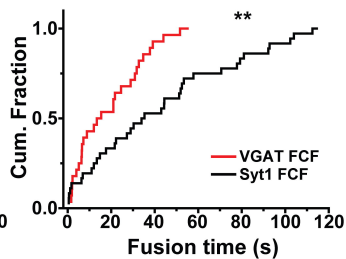
Parvalbumin

Merge

**B****C**

A**B****C**

A**B****C****D**

A**B****C1****C2****C3****D1****D2****E****F****G****H**